Materials & Design 216 (2022) 110573

Contents lists available at ScienceDirect

Materials & Design

journal homepage: www.elsevier.com/locate/matdes

Vacuum-driven assembly of electrostatically levitated microspheres on perforated surfaces

Ward Van Geite [a], Ignaas S.M. Jimidar [a,b,*], Kai Sotthewes [c], Han Gardeniers [b], Gert Desmet [a,*]

[a] Department of Chemical Engineering CHIS, Vrije Universiteit Brussel, Brussels 1050, Belgium
[b] Mesoscale Chemical Systems, University of Twente, Enschede 7522 NB, The Netherlands
[c] Physics of Interfaces and Nanomaterials, University of Twente, Enschede 7522 NB, The Netherlands

HIGHLIGHTS

- An electrostatic cell combined with a vacuum-aspired perforated silicon membrane is designed to arrange dry microspherical powders in ordered two-dimensional geometries.
- By applying strong electric fields, $E \geqslant 1.2$ MV m^{-1}, silica, polystyrene and polymethyl methacrylate (PMMA) with diameters of 5–10 μm are levitated, forming a particle cloud between two electrodes.
- Monodisperse silica or polystyrene particle with a diameter of 5–10 μm are assembled on profiled through-pores spanning an area of at most 2×2 mm^2 on a silicon chip.
- Particle arrays with different geometrical designs are simultaneously assembled in a few seconds.
- As the vacuum-driven force allows releasing the assembled arrays, they are successfully replicated on a polydimethylsiloxane (PDMS) soft surface.

GRAPHICAL ABSTRACT

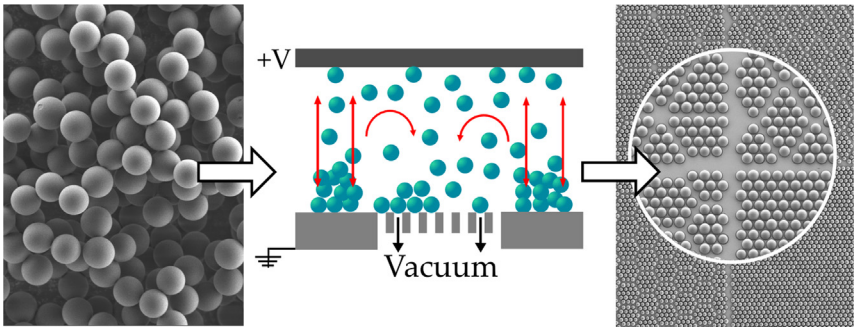

ARTICLE INFO

Article history:
Received 13 December 2021
Revised 18 March 2022
Accepted 18 March 2022
Available online 23 March 2022

Keywords:
Dry particle assembly
Directed assembly
Microspheres

ABSTRACT

At the onset of a miniaturized device era, several promising methods, primarily wet methods, have been developed to attain large-scale assemblies of microparticles. To improve the speed, versatility and robustness of the current methods for the structured assembly of microparticles, an automatable method capable of forming 2D arrays of microspheres on large silicon surfaces is devised. The method uses surfaces perforated with vacuum-suction holes, capable of aspiring and holding individual particles from a particle cloud generated by subjecting a lump of chargeable particles, e.g., silica, polystyrene, and polymethyl methacrylate (PMMA), to a strong electrical field under ambient air conditions. The microsphere levitation depends on the electrical conductivity and permittivity of the particles. A single or double brush stroke can remove excess particles covering the formed arrays. We find that silica or polystyrene

* Corresponding authors at: Department of Chemical Engineering CHIS, Vrije Universiteit Brussel, Brussels 1050, Belgium (I.S.M. Jimidar).
E-mail addresses: i.s.m.jimidar@utwente.nl (I.S.M. Jimidar), gedesmet@vub.be (G. Desmet).

https://doi.org/10.1016/j.matdes.2022.110573

Particle monolayers
Particle transfer

microspheres with a diameter of 5 μm or 10 μm can be assembled on the order of a few seconds, independently of the array size. Owing to the reversible nature of the arresting vacuum force, the assembled layers can be transferred to another surface, such as polydimethylsiloxane (PDMS) sheets, thus providing a key step for future particle printing processes for the fabrication of hierarchical materials, e.g., photonic crystals.

1. Introduction

The perpetual curiosity of scientists to fabricate new materials with pre-engineered structure and properties lies at the heart of the rapidly evolving material science field. In the past decades, scientists have developed a broad diversity of methods to produce close and non-close packed two-dimensional (2D) arrays of micro- or nanoparticles including microgel or hydrogel particles. Such arrays are widely employed in a vast number of applications, such as flexible electronic devices, photonic films, colloidal lithography, microlenses, SERS sensing, fabrication of polymeric sheets and nanomaterials [1–11]. Additionally, 2D arrays can be used as building blocks to engineer three-dimensional particle assemblies using a bottom-up strategy [2,12–16].

Most studies aiming at the production of (self-) assembled particle arrays make use of wet assembly methods, hinging predominantly on a delicate balance of the surface interaction forces and requiring an optimized evaporation rate, solvent properties, pH, temperature [2,17–27]. Consequently, the number of possible particle configurations, e.g, hexagonal and cubic centred arrays, is limited. Furthermore, the slightest imbalance may lead to the formation of cracks and line defects in the assembled array. Dry assembly methods, such as manual rubbing or agitation,[4,17,28–30] have been less intensively explored, despite the higher degree of structural freedom they intrinsically offer. Up to date, the quality of the layers produced with these techniques is highly sensitive to the speed of operation, the applied pressure by the operator during manual rubbing pressure or the occurrence of tribocharging effects. In addition, most successful methods make use of elastomeric substrates,[4,28] making the assembled array prone to deformation during subsequent treatment. On the other hand, Khan and Yoon [17] applied a polymer layer on silicon substrates to attain ordered arrays of silica nanobeads by manual rubbing successfully. Afterwards, the particle array was calcined at a temperature of 500 °C to remove the polymer layer, rendering this method inapplicable to assemble polymer, e.g., polystyrene beads which typically have significantly lower melting temperatures. Thus, a clear impetus remains to develop more robust and automatable assembly methods for a broader spectrum of particle types, i.e., methods less prone to human error or slight deviations from optimized process parameters.

In an attempt to meet this need, the present study explores the possibilities of a new, quick, and upscalable dry assembly technique to produce arrays of precisely positioned microspheres without any constraint on the geometrical pattern or the particle spacing, and without the need for glue to keep the particles in position during subsequent operations [17]. This approach consists of first suspending the particles in an electrostatic cell and then aspiring them by applying a vacuum force onto a silicon membrane that is perforated by an array of through-pores (Fig. 1a). To demonstrate the versatility of the proposed method, experiments were performed using monodisperse silica, polystyrene or polymethyl methacrylate (PMMA) microspheres with a diameter of 5–10 μm. The assembly process on the fabricated perforated devices takes a few seconds, including removing the excess particles using a brush. Since the particles are reversibly captured, the assembled arrays could subsequently be transferred to soft elastomeric surfaces. It is believed this could be a first step towards the 3D printing of functional particle assemblies.

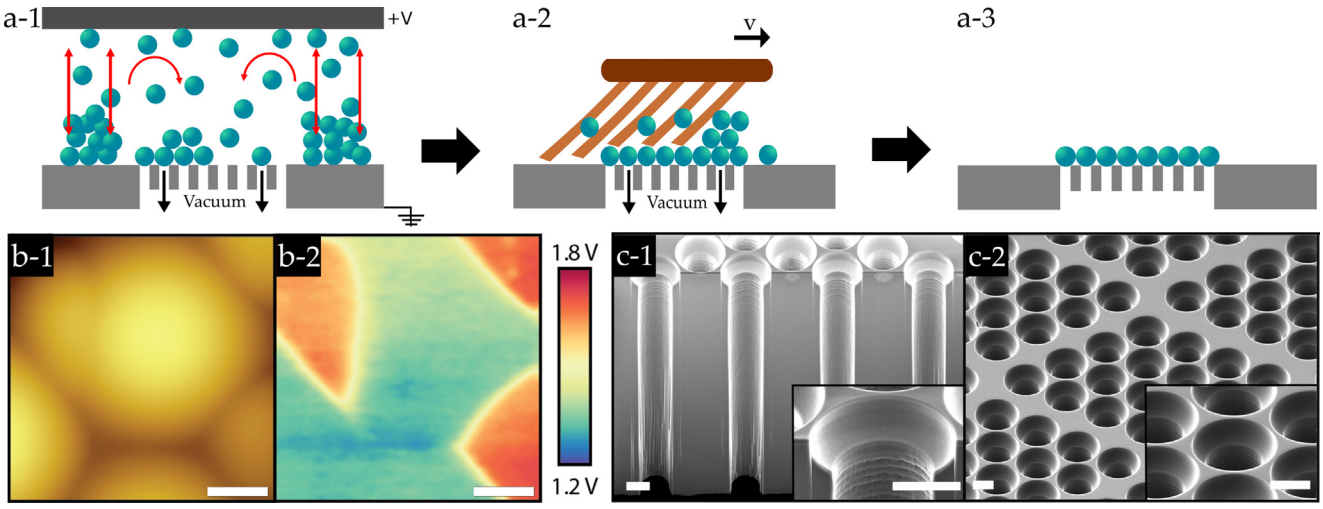

Fig. 1. **(a)** Schematic representation of the experimental setup operating under ambient conditions: **(a-1)** the microspheres deposited next to the through-pores of the perforated silicon membrane are levitated within an electrostatic cell and subsequently guided towards the perforated area on the bottom electrode by applying a vacuum force. The top electrode is connected to a high-voltage potential difference *V*, while the bottom electrode containing the membrane area is grounded. **(a-2)** The excess particles are removed by laterally moving a brush with constant speed v across the assembled array, resulting in a 2D ordered array of microspheres on the membrane surface **(a-3)**. **(b)** The topographic map of a collection of 10 μm silica particles **(b-1)** and the concurrent surface potential map with respect to the tip **(b-2)** obtained using Kelvin probe force microscopy (KPFM) (cf. S1-e). **(c)** SEM images of the cross-section **(c-1)** and a tilted top-view **(c-2)** of the membrane area showing zooms of the funnel-shaped mouth through-pores. Scale bar = 5 μm in all images.

2. Physical mechanism

The microspheres with diameters smaller than 10 μm (ultrafine dry powder) exhibit a relatively large surface to volume ratio, leading to substantially strong cohesive forces over body forces. Consequently, gravity is typically neglected in this respect [31]. In principle, these significantly strong cohesive interactions are challenging as they tend to form agglomerates that challenge the dry assembly process. Therefore, wet assembly methods are preferred over dry techniques to circumvent these cohesive forces.

With regard to the silica microspheres employed in this study, the relevant cohesion forces that may exist among two touching microspheres stem from capillary interactions, van der Waals interactions, and elastic deformations at the point of contact that result in a so-called contact mechanics force [31,32]. From literature it is known that ideally all these cohesive forces depend linearly on the particle's radius $\sim$ R [31,33,32]. Theory predicts that for a 10 μm silica microsphere the van der Waals force is $\approx 10^{-7}$ N, whereas the capillary and contact mechanics force are in the order of $\approx 10^{-6}$ N [31-33]. However, owing to the naturally present roughness on the surface of the microspheres, the real cohesive force among them is significantly reduced. Due to the former, van der Waals interactions are significantly weaker than the other two types of interactions and can be neglected [33].

On the other hand, the capillary interactions are only relevant when hydrophilic bodies, e.g., the silica microspheres, are involved. Under ambient conditions, water vapour inevitably condensates and adsorbs, particularly on these hydrophilic bodies, forming a liquid meniscus between neighbouring particles. Consequently, a capillary force acts among the neighbouring particles, enhancing the cohesion [31].

Next to this capillary force, a contact mechanics force emerges between two touching microspheres which is attributed to their finite elasticity, enhancing the strongly agglomerated state of the silica particles (cf. Fig. S1). To sum up, the capillary force and contact mechanics force are the most dominantly present interaction forces among the silica microspheres, but are reduced to values ($\leqslant 10^{-6}$ N) due to surface irregularities [31,33,34].

The agglomerated state of these microspheres poses a critical challenge for the dry assembly of individual particles into 2D structured arrays. To reduce, for example, the capillary interactions, one could store the silica particles in a humidity-controlled environment, e.g., a glove box, at almost zero humidity for at least four hours. However, this would require including the experimental setup within the glove box and operating the system outside the humidity chamber. The latter is challenging and inefficient at the moment, and therefore a different assembly strategy is preferred.

Inspired by previous studies in which single or weakly agglomerated charged conductive, semiconductive, or dielectric spheres are levitated from electrodes by high electric field strengths [35–38], we recently established that the dielectric silica agglomerates could be disrupted and broken up in individual particles in an electrostatic cell [39]. By performing Kelvin probe force microscopy (KPFM) scans, the contact potential difference V_{CPD} between the particle's surface with respect to the conductive KPFM tip can be measured [29,40]. From the obtained surface potential maps in conjunction with the simultaneously obtained topography maps of the particle surface shown in Fig. 1b, we infer that all the silica particles carry a negative, albeit unevenly distributed, charge (cf. Section S1-e).

In an electrostatic cell, the generated electric field $\vec{E}$ induces a net charge q on the particles present at the top layer of a pile of particles, depending on the permittivity and resistivity of the microspheres. Consequently, a Coulomb force $\vec{F}_C = q\vec{E}$ acts on the charged microspheres [29,36]. In addition, note that the saturation charge that a particle can acquire depends on its surface area $\sim R^2$ and the applied electric field [38]. Exploiting the presence of this charge on the silica particles, it was found that an electric field $\vec{E} \geqslant 1.2$ MV m^{-1} is sufficient to let the induced Coulomb force surpass the cohesion forces namely, the capillary and contact mechanics force, dislodging individual 10 μm silica particles and small agglomerates from the initial particle supply and levitate them opposite the electric field orientation. Furthermore, the study reported that the silica microspheres acquired an average charge q = 2.8 fC,[39] resulting in a Coulomb force F_C in the nN range. In practice, as already stated, the cohesion force among the silica particles is at least one order of magnitude smaller,[33,34] justifying why the 10 μm silica particles should be subjected to high electric field strengths of at least 1.2 MV m^{-1} [33].

When the levitated silica particles and small agglomerates subsequently impact on the top electrode, they can either rebound from, or stick to the top electrode. The latter occurs when the momentum of the particles is too low and the adhesion force with the top electrode is stronger compared to the impact force ($\approx 10^{-6} - 10^{-7}$ N) acting on the microspheres during the collision [39,41]. The other colliding particles, may reduce or change their polarity upon contact with the top electrode, i.e., charge is transferred between the colliding microspheres and the top electrode. Those particles gaining an opposite polarity will move towards the counter electrode, while the other rebounding particles will return to the top electrode. In addition, during these subsequent collisions, most of the smaller agglomerates break up into individual particles. All of the continuously rebounding particles form a particle cloud between the electrodes (cf. Movie S1). Typically, the study of Jimidar et al. found that the lifetime of the particle cloud is between 12 and 15 s [39]. However, as a vacuum force is applied here, particles are attracted towards the membrane, and the cloud's lifetime is reduced. For all the details describing the impact and cloud formation, the reader is kindly referred to the recent study of Jimidar et al. [39].

Note that apart from the strongly agglomerated silica particles, the electrostatic cell could also successfully be used to levitate polystyrene and PMMA microspheres. Even though these microspheres are weakly agglomerated, it proved challenging to levitate and concomitantly form a stable particle cloud between the electrodes. This can be explained by the microspheres' lower conductivity and electrical permittivity than the silica particles. As a result of these electrical properties, the acquired charge on these microspheres is lower amplified by a slower charging process. Consequently, the particles were not immediately levitated, but after about 5 s [38,39].

3. Proposed assembly strategy

Exploiting the possibility of a particle cloud formation between two electrodes,[39] a setup has been designed wherein one of the two electrodes is perforated by an array of through-pores that can be connected to a vacuum or an overpressure (Fig. 1a-1). Immediately after the vacuum force is applied, the electric field is switched on to levitate the monodisperse particles deposited next to the assembly array (cf. Fig. S3). The vacuum force then guides the suspended particles instantaneously i.e., unmeasurably fast with our optical setup towards the through-pores of the membrane surface (cf. Movie S1). Other configurations of the setup (vacuum assembly membrane oriented under 90° or 180°) have been tested and provided similar results provided the electric field points in the right direction (cf. Fig. S2). In the case of the silica particles, an electric field of at least $\vec{E} \geqslant 1.2$ MV m^{-1} was sufficient for the assembly process. In addition, silica particles would be levitated incidentally when lower electric field strengths were applied, however, not

enough to form a stable cloud between the electrodes, i.e., applying lower electric fields results in a low yield of the assembly process.

Microfabrication processing of the perforated silicon devices displayed in Fig. 1c has been performed at the MESA+ nanotechnology institute of the University of Twente. The workflow and fabrication process are presented in section S4 and Fig. S4, respectively. Note that the through-pore size should be smaller than the diameter of the smallest monodisperse particles used in the experiments to prevent clogging of the pores.

To arrange the particles in a different conformation, it suffices to use a differently patterned assembly membrane. On a 4 in. silicon wafer, at least 25 silicon chips carrying various membrane designs can be manufactured in a single run of the fabrication process, which takes approximately three working days. However, we have typically opted for batch processing as it allowed fabricating 25 wafers in six working days. Moreover, after each assembly experiment, the silicon membranes can be recycled and can be used at least 50 times.

4. Results and discussion

4.1. Non-profiled vs profiled through-pores

As shown in Fig. 2a-1,b-1, the high inertial forces resulting from the applied vacuum force prevent the stream of particles to abruptly stop once the holes are filled and, concomitantly, the vacuum force is stopped. Consequently, the array gets covered by excess particles (typical coverage: some 5–30%). The latter can be removed by subsequently brushing across the membrane while maintaining the vacuum force to keep the particles in place (cf. Fig. 1a-3).

Initially, experiments were carried out using membrane pores with a standard cylindrical pore mouth (further referred to as "non-profiled"). This pore type frequently led to a situation wherein some particles ended up on the small ridge between two adjacent pores, presumably because their high inertia causes them to deviate from the airflow streamlines when these locally bend-off to enter one of the through-pores.These misplaced particles inevitably partially block two adjacent pores, such that these pores can continue to attract particles, resulting in the local formation of large clusters (cf. Fig. 2a-1 (red circles) and Fig. S5). To demonstrate these clusters are locally formed and do not pre-exist in the attracted particle cloud, experiments were repeated with a sieve-membrane (13 μm pores) covering the capture membrane and only allowing the passage of single particles (Fig. S6). No difference in cluster formation frequency and magnitude was observed, thus confirming the above hypothesis. Interestingly, the presence of the sieve also did not observably affect the total assembly time (order 1–2 s, mainly determined by the start-up time needed for the particle cloud). Another notable drawback of these standard membrane pores is that they could not hold the correctly positioned particles firmly enough to withstand the high forces acting on them during the subsequent brushing process, i.e., the particles on the pores were mobilized, deteriorating the captured particle array tremendously (cf. the transition from Fig. 2a-1–2a-2).

To overcome both problems, the mouth of the through-pores was profiled by introducing a bowl-shaped funnel structure mark-

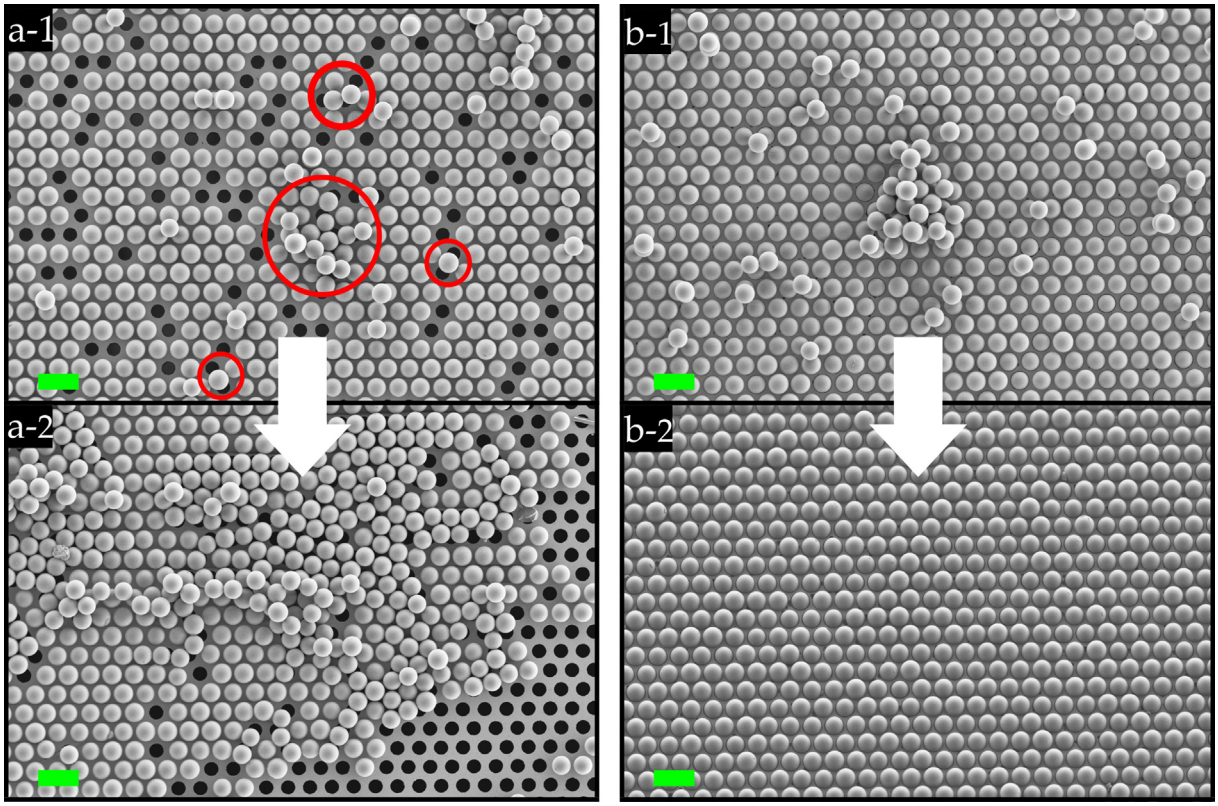

Fig. 2. Representative SEM images of 10 μm silica particle assemblies attained on the silicon membrane areas (1 × 1 mm^2) for the case of **(a)** non-profiled and **(b)** profiled through-pores. The red circles indicate misplaced particles trapped between adjacent pores on the non-profiled membranes. The white arrows indicate the transition before **(1)** and after **(2)** the brushing step. Scale bar = 20 μm.

ing the upper 3 μm (cf. Fig. 1b). This bowl-shaped opening ensures that particles accidentally ending up between two pores will still tip into the pore mouth as this is energetically the most favourable position. These profiled through-pores also more firmly hold the particles in place during the subsequent brushing process (cf. the transition from Fig. 2b-1–2b-2).

4.2. Optimize assembly process

Next to the presence of excess particles, another regularly observed defect is the occurrence of vacancies. As it can be argued the latter might be attributed to a too strong loss in aspiration force near the end of the filling process, when only a few pores remain open, the effect of the applied pressure difference ΔP was investigated (Fig. 3a). As can be noted from the blue bar segments, the number of vacant pores significantly reduces when increasing the pressure difference, reaching an average level of 1–2 vacant pores on a total of 8000 through pores when $\Delta P \geqslant 500$ mbar. These results can possibly be explained by the fact that the force exerted on the particles by vacuum pressures of $\Delta P \geqslant 500$ mbar is approximately $\approx 10^{-5} - 10^{-6}$ N, which is larger than the contact force of a colliding particle ($\approx 10^{-6} - 10^{-7}$ N) discussed in Section 2.

Using a high ΔP also clearly increases the number of excess particles (orange segments in Fig. 3a), but these can be removed using a cleaning step (cf. the transition from Fig. 3a and b). We have used different brushes, e.g., antistatic brushes with stiff hairs, to remove the excess particles. The best excess particle removal results were obtained using a high hair density brush (cf. S1-d) moving with a constant velocity v across the particle assembly (cf. Movie S2). The occasional extra vacancies introduced by this step were especially found in the first row of particles addressed by the brush (cf. Fig. S7). As the outer membrane rows are particularly difficult to etch and therefore have a much higher frequency of partially closed through-pores, the edges were excluded from the data in Figs. 3b and c. Fig. 3b groups all high velocity brushing results (v = 120 mms^{-1}, single sweep). The strong reduction of the orange bar segments observed when moving from Fig. 3a and b shows that under these brushing conditions most excess particles were removed. The blue bar segments however also indicate a significant number of new vacancies is created when $\Delta P \leq 150$ mbar.

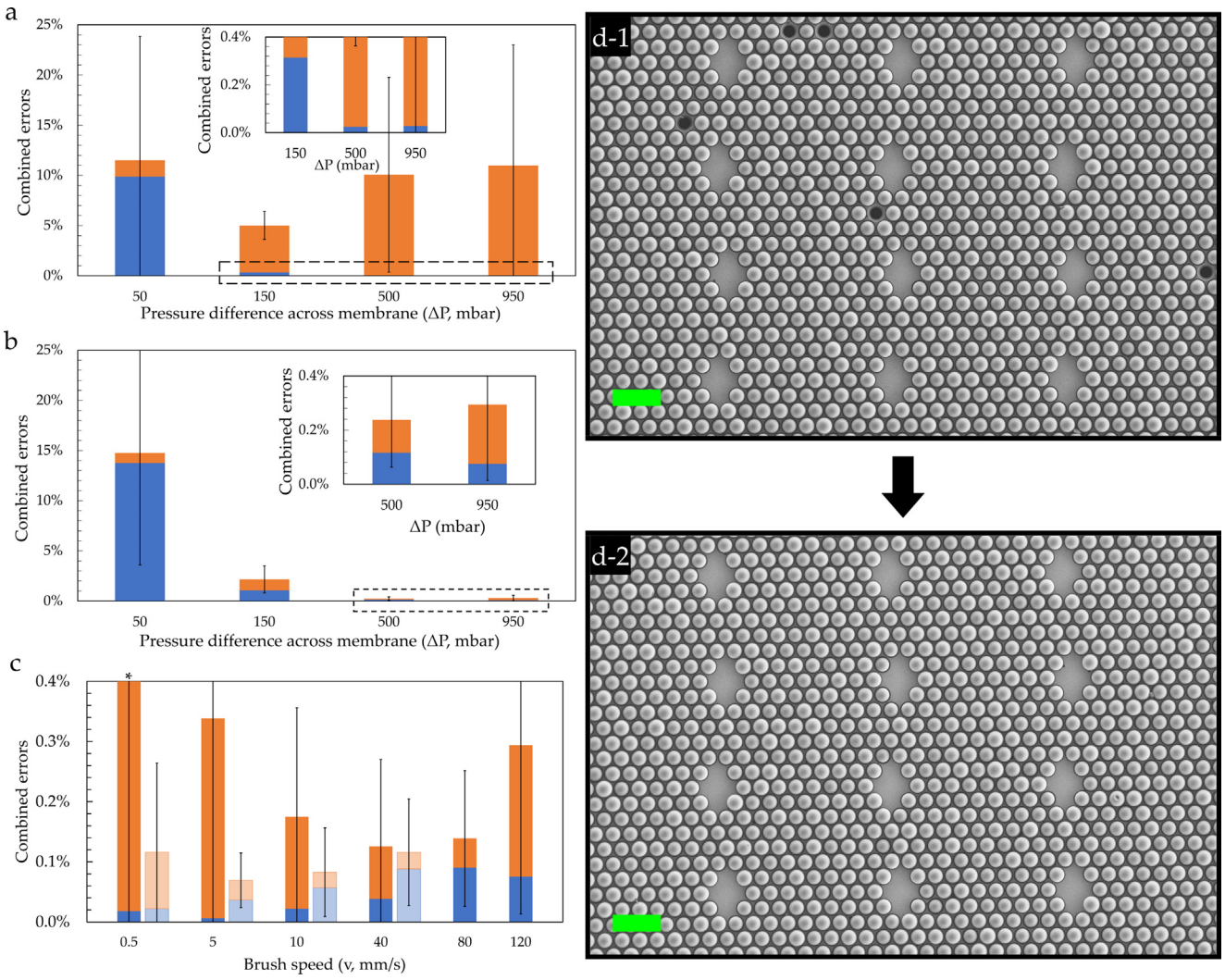

Fig. 3. Bar chart of the combined errors (vacancies = blue and excess particles = orange) for 10 μm silica particle assembled on 1 × 1 mm^2 membranes with profiled through-pores as a function of the applied pressure difference ΔP **(a)** before and **(b)** after a brushing step with speed v = 120 mm/s. **(c)** Effect of brushing speeds v and number of brushing steps (1 × for solid-coloured bars or 2 × for transparent bars) at ΔP = 950 mbar. Second sweep with the brush perpendicular to the first brushing direction. The * represents a value of 4.0 ± 4.7%. **(d)** SEM images of a 10 μm silica particle array **(d-1)** before and **(d-2)** after a refill step. The dark spots appearing in **(d-1)** are vacant pores. Scale bar = 30 μm.

However, it is noteworthy that occasionally a few vacancies were filled with microspheres during the brushing step.

Next, different brushing velocities were explored at the maximal ΔP = 950 mbar. Both single sweep and double sweep experiments (2^{nd} sweep carried out by turning sample 90°) were considered. They are respectively represented by the solid and the transparent bars in Fig. 3c. As can be noted, the number of defects goes through a clear optimum in both the single and the double sweep case, with the optimum shifting from v = 40 mm s^{-1} for a single sweep cleaning to a lower brushing velocity (v = 5 mm s^{-1}) in case of a double sweep cleaning. If the brushing velocity is too low, excess particles are insufficiently removed, while for velocities past the optimum the brushing speed is so high that the cleaning step creates additional vacancies. The 0.03% occurrence of vacancies and excess particles observed for the v = 5 mm s^{-1} brushing velocities corresponds to only 2 misplaced or missing particles on a total of 8000 pores. Probably, these few defects can be attributed to the presence of dust particles (all experiments were conducted in an ordinary chemical lab lacking air filtering) or etching remnants inside the pores.

It was also investigated whether the creation and occurrence of vacancies could be countered by adding an extra filling step. This was done at ΔP = 950 mbar and v = 10 mms^{-1}. As displayed in Fig. 3d, this refilling approach can indeed be successfully used to fill the last remaining vacancies.

As a final note on the brushing process, the setup is currently limited to realizing a perfect brush alignment with respect to the first assembled particle layer on the membrane. This could improve the brushing process by lowering the risk of removing precisely positioned particles from the membrane pores.

4.3. Assembly of different types of particles on various membrane designs

An advantage over most previously proposed assembly methods,[1,2,5,20,28] is that the presently proposed method allows to arrange the particles in any desired 2D pattern of non-closely packed particles and even combinations thereof (Fig. 4). To demonstrate its applicability to different sizes, Fig. 4b show successful assembly of 5 μm silica particles in lieu of 10 μm particles. The proposed approach also works equally well on membranes spanning either a larger or a smaller area (Figs. 4b-2 and S8). The method's versatility is further demonstrated by applying it to other polarizable particles, such as polystyrene particles (cf. Fig. 4c) and PMMA microspheres (cf. S9). A caveat here is that for the polystyrene and PMMA microspheres, electric fields of approximately $\vec{E} \geqslant 2.5$ MV m^{-1} were required to levitate these microspheres, with the complete assembly process, including brushing steps, lasting for 10 s. The stronger electric fields and longer waiting times for particle levitation can be explained by the lower electrical conductivity and permittivity of the particles [39].

In the present study, we solely studied the assembly of 5 and 10 μm particles using the proposed method.In principle, the method can be relatively easily extended to smaller sized particles after adjusting the pore diameter of the perforated device. However, it can be expected that, when going towards sub-

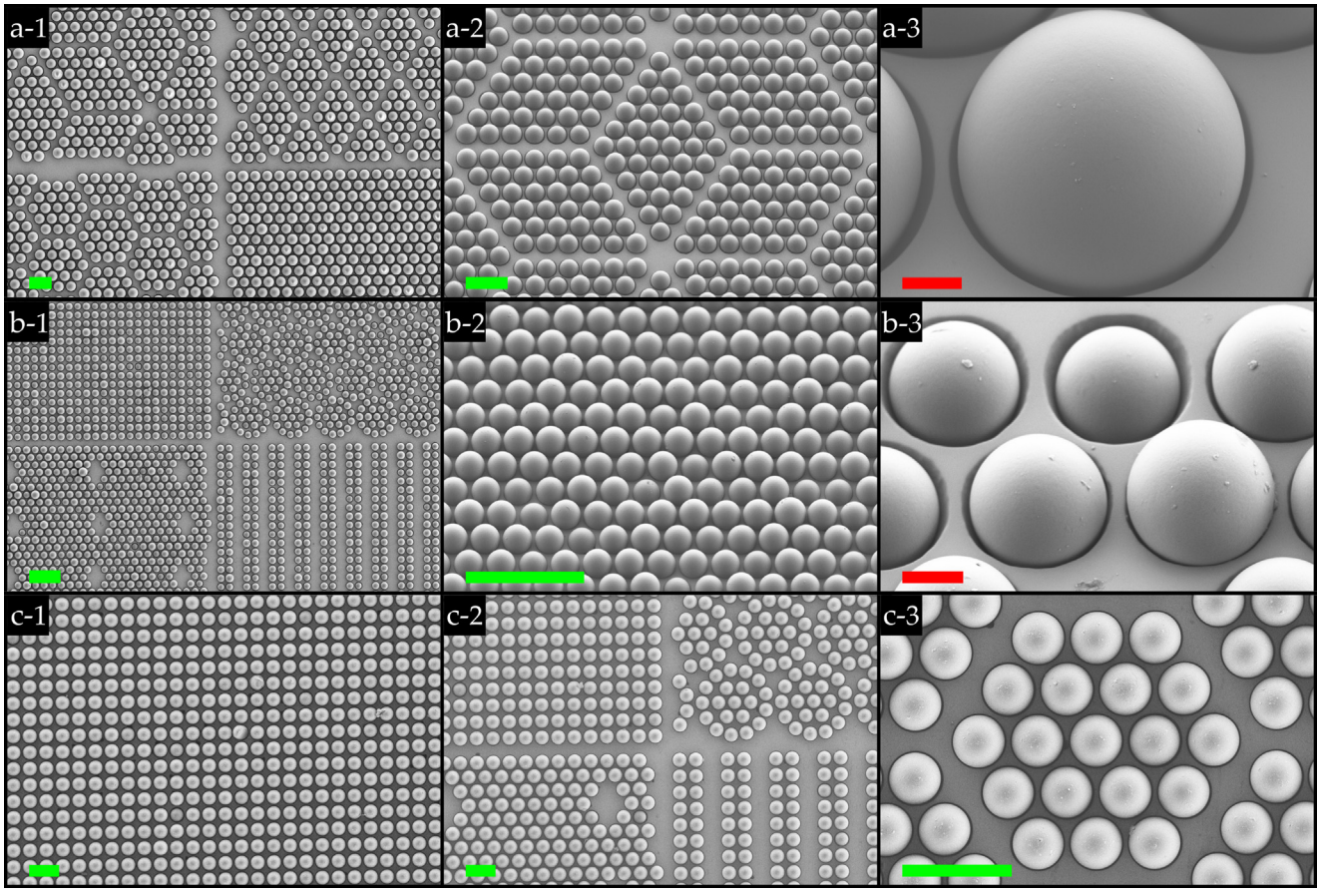

Fig. 4. SEM images of 2D particle array arrangements with different designs, attained with: **(a)** silica microspheres with a diameter of 10 μm and **(b)** 5 μm; and **(c)** polystyrene microspheres with a diameter of 10 um. The distance d between neighbouring particles is **(a & c)** d = 1.25 um and **(b)** d = 0.63 μm. All images were obtained on 1 × 1 mm^2 profiled membranes, except in **(b-2)** where the membrane area was 2 × 2 mm^2 (cf. Fig. S8) Scale bar: green = 20 μm; red = 2 μm.

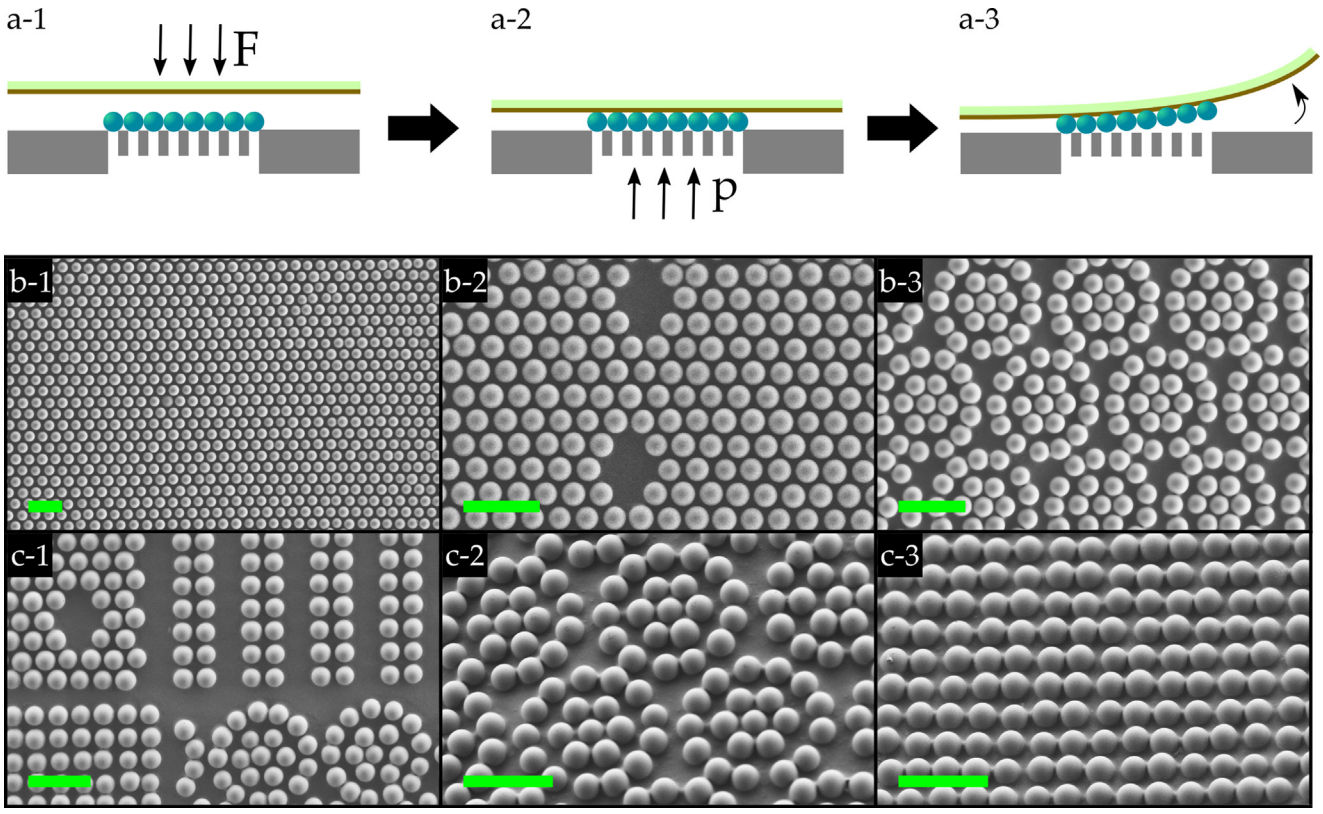

Fig. 5. **(a)** Schematic representation of the process used to transfer the particles from the silicon membranes onto a soft elastomeric surface carrying an adhesive layer, comprised of **(a-1)** manually pressing the adhesive layer against the assembled array with a force *F*; **(a-2)** application of an overpressure p across the membrane through-pores (typically p = 4–7 bar), and **(a-3)** gently peeling off the elastomeric surface containing the transferred particles. SEM images of the transferred 10 μm silica particle arrays on **(b)** carbon tape and **(c)** a 30:1 PDMS sheet with a thickness of 600 μm attached onto a microscope glass. Scale bar is 30 μm.

micrometer or nanoparticles, the interparticle forces, e.g., the van der Waals forces, could dominate such that clusters of particles will already be formed, reducing the quality of the assembled array of particles. Furthermore, as the size of the microspheres is reduced, the induced charge on the particle's surface will be lower (cf. Section 2), making the electrical levitation of particles more challenging. The assembly of nanoparticles hence remains to be studied. In addition, instead of the conventional photolithography techniques used here, alternative sub-micron patterning techniques, e.g., e-beam lithography should be applied, to produce perforated devices for the assembly of colloidal particles.

It is noteworthy that another defect might occur during the assembly process in case of a polydisperse sample of particles. Here, we presented assembled particles arrays with a pitch of 1.25 μm. If in this case an oversized particle with a of diameter in excess of 1.2 times the average diameter would be captured, it would block neighbouring pores from capturing other particles, i.e., the neighbouring pores would be vacant. We have used highly monodisperse particles such that this effect can be neglected. However, when employing polydisperse particles with, for example, a relative standard deviation > 10%, this effect should be taken into account, as the probability for blocked pores is already ≈ 2%. Moreover, when one would desire assemblies with a smaller pitch, or even closely-packed arrangements, the dispersity of the particles will be crucial, i.e., highly monodisperse particles would be needed. In the latter case, one would even need equal sized-particles.

4.4. Transfer of assembled arrays

Exploiting the reversible nature of the vacuum force, the assembled particle arrays can be transferred onto an adhesive elastomeric surface, such as carbon tape or polydimethylsiloxane (PDMS) sheets. In the latter case, a thin 30:1 PDMS sheet (600 μm thick) acting as the adhesive layer was attached to a microscope glass, preventing the PDMS surface from extensive deformation that may disturb the transfer process. As illustrated in Fig. 5a, the soft surface is first gently pressed on the membrane to promote the adhesion with the particles, and subsequently, an over-pressure (order 4–7 bar) is applied to ensure that all particles are transferred to the adhesive surface. Next, the soft surface carrying the transferred array is slowly detached from the membrane, keeping the particles in place on the transferred substrate. Figs. 5-b-c show the mutual distances between the particles remain intact after their transfer to the adhesive surface.

5. Conclusions

By electrostatically levitating 5–10 μm silica, polystyrene, and PMMA microspheres and simultaneously attracting them on membrane surfaces using a vacuum-driven force, a new route is presented for the dry assembly of non-closely packed microspheres. The obtained results highlight the versatility of the proposed method, which solely uses a sufficiently strong vacuum force to rapidly capture and assemble the suspended particles on any predetermined lattice position on the profiled through-pores of the silicon membranes. The speed of the method (order of a few seconds to complete the aspiration and cleaning steps) is independent of the size of the array. However, as the electrical permittivity and conductivity of the polystyrene and PMMA microspheres are lower compared to the silica microspheres, the efficiency of the particle levitation and assembly speed drops. Consequently, the duration of the assembly process is approximately 10 s for the polystyrene

and PMMA microspheres. In addition, a critical aspect of the proposed approach is the requirement to work under dust-free conditions. The method further encompasses a brushing step to remove the inevitable excess particles from the secured particle array. As the assembled arrays are maximally accessible, they can potentially be functionalized to change their property depending on the application at hand, e.g., to manufacture Janus particles for catalytic purposes, or coated with DNA strains. Additionally, it has been demonstrated that particle assemblies can be transferred successfully to an adhesive elastomeric surface by reversing the applied pressure across the membranes. Therefore, we believe that the proposed method, making a unique combination of electrical (to break the particle agglomerates and suspend them in the air) and vacuum forces, may enable new particle printing processes for the production of 2D (e.g., soft electronic or wearable devices, photonic crystals) and potentially even 3D hierarchical materials (cf. layer-by-layer addition). We also believe the present approach is also more amenable to automatization than the more wet and dry assembly techniques described in literature until now.

Declaration of Competing Interest

The authors declare that they have no known competing financial interests or personal relationships that could have appeared to influence the work reported in this paper.

Acknowledgement

The authors gratefully acknowledge funding from the ERC Advanced Grant "PrintPack" (No. 695067).

Appendix A. Supplementary material

Experimental details, additional data, figures, and movies available in Supporting Information. Supplementary data associated with this article can be found, in the online version, at https://doi.org/10.1016/j.matdes.2022.110573.

References

[1] H. Hwang, U. Jeong, Microparticle-based soft electronic devices: toward one-particle/one-pixel, Adv. Funct. Mater. (2019) 1901810.
[2] N. Vogel, M. Retsch, C.-A. Fustin, A. del Campo, U. Jonas, Advances in colloidal assembly: the design of structure and hierarchy in two and three dimensions, Chem. Rev. 115 (13) (2015) 6265–6311.
[3] G. Chu, F. Chen, B. Zhao, X. Zhang, E. Zussman, O.J. Rojas, Self-assembled nanorods and microspheres for functional photonics: Retroreflector meets microlens array, Adv. Opt. Mater. 9 (9) (2021) 2002258.
[4] K. Koh, H. Hwang, C. Park, J.Y. Lee, T.Y. Jeon, S.-H. Kim, J.K. Kim, U. Jeong, Large-area accurate position registry of microparticles on flexible, stretchable substrates using elastomer templates, ACS Appl. Mater. Interf. 8 (41) (2016) 28149–28158.
[5] Y. Wang, M. Zhang, Y. Lai, L. Chi, Advanced colloidal lithography: from patterning to applications, Nano Today 22 (2018) 36–61.
[6] Y. Wang, Y. Yu, J. Guo, Z. Zhang, X. Zhang, Y. Zhao, Bio-inspired stretchable, adhesive, and conductive structural color film for visually flexible electronics, Adv. Funct. Mater. 30 (32) (2020) 2000151.
[7] M. Boularas, S. Radji, E. Gombart, J.-F. Tranchant, V. Alard, L. Billon, Functional film by trigger-free self-assembly of adhesive soft microgels at skin temperature, Mater. Des. 147 (2018) 19–27.
[8] D.A. Foster, D.K. Hwang, Microfluidic flow assembly system with magnetic clamp for unlimited geometry in millimetric hydrogel film patterning, Appl. Mater. Today 26 (2022) 101330.
[9] G.R. Hendrickson, M.H. Smith, A.B. South, L.A. Lyon, Design of multiresponsive hydrogel particles and assemblies, Adv. Func. Mater. 20 (11) (2010) 1697–1712.
[10] C. Song, B. Ye, J. Xu, J. Chen, W. Shi, C. Yu, C. An, J. Zhu, W. Zhang, Large-area nanosphere self-assembly monolayers for periodic surface nanostructures with ultrasensitive and spatially uniform sers sensing, Small 18 (8) (2022) 2104202.
[11] M.Z. Iqbal, I. Ali, W.S. Khan, X. Kong, E. Dempsey, Reversible self-assembly of gold nanoparticles in response to external stimuli, Mater. Des. 205 (2021) 109694.
[12] Y.A. Vlasov, X.-Z. Bo, J.C. Sturm, D.J. Norris, On-chip natural assembly of silicon photonic bandgap crystals, Nature 414 (6861) (2001) 289–293.
[13] H.-N. Barad, H. Kwon, M. Alarcón-Correa, P. Fischer, Large area patterning of nanoparticles and nanostructures: current status and future prospects, ACS Nano 15 (4) (2021) 5861–5875.
[14] Z. Cai, Z. Li, S. Ravaine, M. He, Y. Song, Y. Yin, H. Zheng, J. Teng, A. Zhang, From colloidal particles to photonic crystals: advances in self-assembly and their emerging applications. In: Cai, Zhongyu and Li, Zhiwei and Ravaine, Serge and He, Mingxin and Song, Yanlin and Yin, Yadong and Zheng, Hanbin and Teng, Jinghua and Zhang, (eds) Royal Society of Chemistry. Ao Chem. Soc. Rev. 50 (10) (2021) 5898–5951.
[15] M. Dijkstra, E. Luijten, From predictive modelling to machine learning and reverse engineering of colloidal self-assembly, Nat. Mater. 20 (6) (2021) 762–773.
[16] J. Wang, P.W. Pinkse, L.I. Segerink, J.C. Eijkel, Bottom-up assembled photonic crystals for structure-enabled label-free sensing, ACS Nano (2021).
[17] N.N. Khanh, K.B. Yoon, Facile organization of colloidal particles into large, perfect one-and two-dimensional arrays by dry manual assembly on patterned substrates, J. Am. Chem. Soc. 131 (40) (2009) 14228–14230.
[18] J. Aizenberg, P.V. Braun, P. Wiltzius, Patterned colloidal deposition controlled by electrostatic and capillary forces, Phys. Rev. Lett. 84 (13) (2000) 2997.
[19] T. Kraus, L. Malaquin, E. Delamarche, H. Schmid, N.D. Spencer, H. Wolf, Closing the gap between self-assembly and microsystems using self-assembly, transfer, and integration of particles, Adv. Mater. 17 (20) (2005) 2438–2442.
[20] C. Lipp, K. Uning, J. Cottet, D. Migliozzi, A. Bertsch, P. Renaud, Planar hydrodynamic traps and buried channels for bead and cell trapping and releasing, Lab Chip (2021).
[21] N. Berneman, I.S. Jimidar, W. Van Geite, H. Gardeniers, G. Desmet, Rapid vacuum-driven monolayer assembly of microparticles on the surface of perforated microfluidic devices, Powder Technol. 390 (2021) 330–338.
[22] Y. Yin, Y. Lu, B. Gates, Y. Xia, Template-assisted self-assembly: a practical route to complex aggregates of monodispersed colloids with well-defined sizes, shapes, and structures, J. Am. Chem. Soc. 123 (36) (2001) 8718–8729.
[23] R. McGorty, J. Fung, D. Kaz, V.N. Manoharan, Colloidal self-assembly at an interface, Materials Today 13 (6) (2010) 34–42.
[24] C.D. Díaz-Marín, R.M. Shetty, S. Cheung, G. Vaartstra, A. Gopinath, E.N. Wang, Rational fabrication of nano-to-microsphere polycrystalline opals using slope self-assembly, Langmuir 37 (43) (2021) 12568–12576.
[25] B. Perkins-Howard, A.R. Walker, Q. Do, D.I. Senadheera, F. Hazzazi, J. Grundhoefer, T. Daniels-Race, J.C. Garno, Surface wettability drives the crystalline surface assembly of monodisperse spheres in evaporative colloidal lithography, J. Phys. Chem. C (2022).
[26] A. Hensley, W.M. Jacobs, W.B. Rogers, Self-assembly of photonic crystals by controlling the nucleation and growth of dna-coated colloids, PNAS 119 (1) (2022).
[27] V. Lotito, T. Zambelli, Approaches to self-assembly of colloidal monolayers: a guide for nanotechnologists, Adv. Colloid Interface Sci. 246 (2017) 217–274.
[28] C. Park, T. Lee, Y. Xia, T.J. Shin, J. Myoung, U. Jeong, Quick, large-area assembly of a single-crystal monolayer of spherical particles by unidirectional rubbing, Adv. Mater. 26 (27) (2014) 4633–4638.
[29] I. Jimidar, K. Sotthewes, H.J. Gardeniers, G. Desmet, Spatial segregation of microspheres by rubbing-induced triboelectrification on patterned surfaces, Langmuir 36 (24) (2020) 6793–6800.
[30] Y. Wang, X.Y. Wei, S.Y. Kuang, H.Y. Li, Y.H. Chen, F. Liang, L. Su, Z.L. Wang, G. Zhu, Triboelectrification-induced self-assembly of macro-sized polymer beads on a nanostructured surface for self-powered patterning, ACS Nano 12 (1) (2018) 441–447.
[31] H.-J. Butt, M. Kappl, et al., Surface and Interfacial Forces, Wiley Online Library, 2010.
[32] J.N. Israelachvili, Intermolecular and Surface Forces, Academic Press, 2011.
[33] I.S.M. Jimidar, Microsphere handling at the microscale: New tools and new effects, Ph.D. thesis, University of Twente, 2021.
[34] R. Jones, H.M. Pollock, J.A. Cleaver, C.S. Hodges, Adhesion forces between glass and silicon surfaces in air studied by afm: effects of relative humidity, particle size, roughness, and surface treatment, Langmuir 18 (21) (2002) 8045–8055.
[35] A. Cho, Contact charging of micron-sized particles in intense electric fields, J. Appl. Phys. 35 (9) (1964) 2561–2564.
[36] M. Shoyama, S. Nishida, S. Matsusaka, Quantitative analysis of agglomerates levitated from particle layers in a strong electric field, Adv. Powder Technol. 30 (10) (2019) 2052–2058.
[37] T. Pähtz, H.J. Herrmann, T. Shinbrot, Why do particle clouds generate electric charges?, Nat Phys. 6 (5) (2010) 364–368.
[38] Y. Wu, G.P. Castle, I. Inculet, S. Petigny, G. Swei, Induction charge on freely levitating particles, Powder Technol. 135 (2003) 59–64.
[39] I.S. Jimidar, K. Sotthewes, H. Gardeniers, G. Desmet, A detailed study of the interaction between levitated microspheres and the target electrode in a strong electric field, Powder Technol. 383 (2021) 292–301.
[40] W. Melitz, J. Shen, A.C. Kummel, S. Lee, Kelvin probe force microscopy and its application, Surf. Sci. Rep. 66 (1) (2011) 1–27.
[41] C. Thornton, Z. Ning, A theoretical model for the stick/bounce behaviour of adhesive, elastic-plastic spheres, Powder Technol. 99 (2) (1998) 154–162.